Flow Induction by Rotary Jets

Kurt H. Hohenemser*
McDonnell Aircraft Corporation, St. Louis, Mo.

Flow induction by rotary jets is analyzed under the assumption that the flow interaction consists of a first phase with mutual isentropic deflection of steady flows in a rotor-fixed frame of reference and a second phase with constant area mixing of the two flows. The relative importance of these two phases for the over-all performance of the flow inductor depends largely on the temperature ratio of the primary and secondary gas. For a numerical example the analytical results are compared with flow induction experimental results taken at equal gas temperature.

Nomenclature

v	=	velocity
u	=	velocity in rotating frame of reference
A	=	flow area
ρ	=	density
m	=	total mass flow
c_p, c_v	=	specific heats at constant pressure and at constant volume, respectively
$\gamma = c_p/c_v$	=	specific heat ratio
M	=	Mach number
p	=	static pressure
T	=	absolute temperature
η	=	turbofan efficiency
τ	=	flow induction efficiency
F	=	thrust
β	=	angle between axial direction and flow direction in tangential plane
ϕ	=	potential energy of centrifugal field

Subscripts

p	=	primary
s	=	secondary
o	=	freestream
i	=	inlet
d	=	end of deflection
e	=	exit
t	=	tangential

Superscripts

o	=	stagnation temperatures or pressures
(′)	=	primary or secondary flow state after isentropic expansion from inlet total pressure to exit static pressure
(–)	=	nondimensional variables using v_p', ρ_p', $(\rho_p' v_p'^2/2)$, T_p', A_p', m_p as reference values, respectively, for velocity, density, pressure, temperature, area, and mass flow

1. Introduction

FLOW induction, which is widely used in simple pumping and jet thrust augmentation devices, has recently attracted considerable attention in the aerospace field for applications to airplane vertical flight and to space vehicle launching. In ejectors, flow induction of a secondary low-velocity gas by a primary high-velocity gas is essentially achieved by shear forces between the two flows. Flow induction is theoretically more efficient by pulsing flows or pressure waves. A third type of flow induction avoids both the necessity of the bulky mixing ducts of ejectors and the intricacies of pulsing flows. Instead, rotary primary jets are interacting with the secondary flow in a flow pattern that is steady in a rotating frame of reference, whereby part of the axial momentum and energy transfer from the primary jets to the secondary flow is accomplished through fluid interface pressure forces rather than through shear forces. In previous theories of this type of flow induction, Foa,[1–4] Hohenemser,[5] and Cox and Campbell,[6] mixing effects are either neglected or mixing is assumed to take place at the exit static pressure, which does not modify the performance of the device. In ejectors, mixing is usually achieved at constant flow area. Therefore, in order to obtain a comparison with the ejector, it is assumed in the following study that the transfer of axial momentum and of energy by fluid interface pressure forces is followed by mixing of the two flows at constant area. The study is limited to subsonic speeds of the mixed flow. It is assumed that primary and secondary flow consist of the same ideal gas with constant specific heats, but with different inlet stagnation temperatures and pressures. In the limit of zero rotational speed of the primary jets, the analysis reduces to that of the ideal constant area ejector presented for incompressible flow by McClintock and Hood[7] and extended to compressible flow by Rabeneck, Shumpert, and Sutton.[8] Refinements of the analysis from consideration of exit flow nonuniformities and from wall friction as they are treated by Mitchell[9] and by Traksel[10] have been omitted from this paper in order to bring out better the basic effects of rotary jets. For the same reason, the effects of diffusers, which are discussed extensively by Payne,[11] have been omitted.

Received January 18, 1965; revision received May 19, 1965. The work was performed at and sponsored by McDonnell Aircraft Corporation, while the author was associated with this corporation. The tests were supervised by Mirko Bolanovich and Hershel Sams. The numerical evaluation was performed by John L. Porter.

* Senior Scientist; now Professor of Aerospace Engineering, Washington University, St. Louis, Mo. Associate Fellow Member AIAA.

2. Flow Induction Performance Measures

2.1. Exit Velocity

The difficulty in defining flow induction performance lies in the nonuniformity of the exit flow. The mass flow, the momentum, and the kinetic energy flow are proportional, respectively, to the velocity average, the velocity square average, and the velocity cube average, which in general define different velocity means. Fortunately, it is an experimental fact that for well-designed flow induction devices these three velocity means are close to each other, so that in the first approximation their differences can be neglected. For ejectors with a cylindrical mixing section and with a single central primary jet, this condition is obtained for a mixing section length-to-diameter ratio of 8 to 10.[9] For the rotary jet flow inductor of the type shown in Fig. 1, model experiments indicated that this condition is obtained already for interaction duct length-to-diameter ratios of 1 to 2. In the following analysis, the three exit velocity averages are assumed to be identical, so that the mass flow is proportional to v_e, the momentum flow is proportional to v_e^2, and the kinetic energy flow is proportional to v_e^3; the velocity v_e being the average determined from mass flow m, exit flow area A_e, and density ρ_e by $v_e = m/A_e\rho_e$. Although this assumption cannot be expected to hold in general, it is a reasonable approximation for well-designed flow induction devices.

Assuming that there is no heat exchange between the flows and the environment during the time that they pass through the flow inductor, one can establish a relation between the average exit velocity v_e, the exit area A_e, and the mass flow ratio m_s/m_p, which is valid no matter what the mechanism or the efficiency of the energy transfer between the two flows. Nondimensional variables, indicated by a bar, will be referred to the condition of the primary flow when expanded isentropically to the exit static pressure. Reference values for velocity, density, pressure, temperature, flow area, and mass flow are, respectively, v_p', ρ_p', $(\rho_p' v_p'^2/2) = (\gamma p_e M_p'^2/2)$, T_p', A_p', and m_p. The energy equations for the reference flow and for the exit flow

$$v_p'^2/2c_p = T_{pi}^0 - T_p' \tag{1}$$

$$v_e^2/2c_p = T_e^0 - T_e \tag{1a}$$

can be combined into the single nondimensional equation

$$\bar{v}_e^2 = (\bar{T}_e^0 - \bar{T}_e)/(\bar{T}_{pi}^0 - 1) \tag{2}$$

The equation of state and the continuity equation of the exit flow

$$\bar{T}_e = 1/\bar{\rho}_e \qquad \bar{m} = \bar{\rho}_e \bar{v}_e \bar{A}_e$$

can be combined into the equation

$$\bar{T}_e = \bar{v}_e \bar{A}_e/\bar{m} \tag{3}$$

and the assumed absence of heat exchange with the environment is expressed by

$$\bar{T}_e^0 = (1/\bar{m})\bar{T}_{pi}^0 + (m_s/m)\bar{T}_{si}^0 \tag{4}$$

Inserting Eqs. (3) and (4) into Eq. (2), one obtains a quadratic equation for the exit velocity $\bar{v}_e$:

$$\bar{v}_e^2 \bar{m}(\bar{T}_{pi}^0 - 1) + \bar{v}_e \bar{A}_e = \bar{T}_{pi}^0 + \bar{m}_s \bar{T}_{si}^0 \tag{5}$$

The negative root has no physical significance, and the mixed exit flow velocity depends uniquely on the inlet total nondimensional temperatures, on the area ratio, and on the mass flow ratio and is independent of the flow induction efficiency. According to the definition of $\bar{T}_{pi}^0$, the inlet total nondimensional temperature of the primary flow is connected with the primary flow pressure ratio by the isentropic relation:

$$p_{pi}^0/p_e = (\bar{T}_{pi}^0)^{\gamma/(\gamma-1)} \tag{6}$$

For a typical numerical example, which will be used throughout this paper, two curves of exit velocity ratio v_e/v_p' vs mass flow ratio m_s/m_p according to Eq. (5) are shown in Fig. 2. The area ratio for this example is $A_e/A_p' = 16$, the primary pressure ratio is $p_{pi}^0/p_e = 2.8$, and the specific heat ratio is $\gamma = 1.4$. The two solid curves in Fig. 2 refer to total inlet temperature ratios of $T_{pi}^0/T_{se}^0 = 1$ and 4. The dash curves in Fig. 2 will be discussed later.

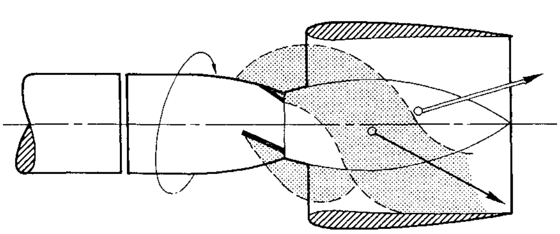

Fig. 1 Schematic of a rotary jet flow induction device.

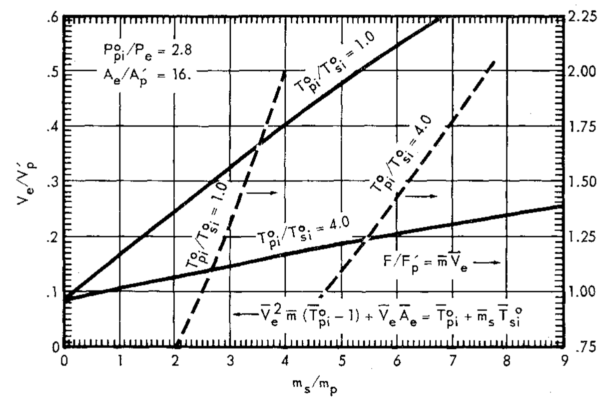

Fig. 2 Exit velocity ratio and static thrust augmentation ratio.

2.2 Flow Induction Efficiency

A variety of flow induction efficiency measures have been devised and used. As long as one is merely interested in comparing various flow induction devices among each other, it is not important which of the various efficiency concepts one selects. However, under certain conditions, the flow inductor is competitive with the most sophisticated fluid energy transformer, the turbofan, and therefore it would seem desirable to use the type of efficiency customarily applied to turbomachinery. The efficiency of a turbofan is usually defined by the enthalpy increase of the secondary flow from isentropic compression between total inlet and total exit pressure divided by the enthalpy decrease of the primary flow for isentropic expansion between total inlet and total exit pressure:

$$\eta = (m_s/m_p)(T_s^{0\prime} - T_{si}^0)/(T_{pi}^0 - T_p^{0\prime}) \tag{7}$$

A more convenient measure, which for flow inductors is in most cases almost numerically identical to η, is the kinetic efficiency defined by the increase in kinetic energy of the secondary flow over the loss of kinetic energy of the primary flow, all kinetic energies taken at static exit pressure p_e:

$$\tau = (m_s/m_p)(\bar{v}_e^2 - \bar{v}_s'^2)/(1 - \bar{v}_e^2) \tag{8}$$

The exit velocity $\bar{v}_e$ is computed from Eq. (5), and v_s' is the secondary flow velocity for isentropic expansion from total inlet pressure to static exit pressure:

$$\bar{v}_s'^2 = (\bar{T}_{si}^0 - \bar{T}_s')/(\bar{T}_{pi}^0 - 1) \tag{9}$$

with

$$T_{si}^0/T_s' = (p_{si}^0/p_e)^{(\gamma-1)/\gamma} \tag{10}$$

For augmenter operation, when $p_e \lessapprox p_{si}^0$, v_s' represents the freestream velocity of the secondary flow. For pumping operation, when $p_e > p_{si}^0$, the term $\bar{v}_s'^2$ will assume, according to Eqs. (9) and (10), a negative value. It then represents a difference in pressure energy rather than in kinetic energy. The advantage of τ over η lies in the fact that τ merely requires the knowledge of the static exit pressure, which is usually directly given, whereas η requires the knowledge of the total exit pressures of the two flows if they were to be discharged unmixed with identical exit velocity v_e, which requires a somewhat involved computation. For incompressible flows η and τ are identical. For compressible flows the deviations between η and τ are small if the difference between the static pressures at merging and at the duct exit is small, a condition that is usually satisfied for flow inductors. The two flows can then be treated during their interaction as approximately incompressible although their densities may be quite different from each other.

The customary way of presenting flow inductor performance data is in the form of an operating line that shows the exit static pressure over secondary inlet total pressure:

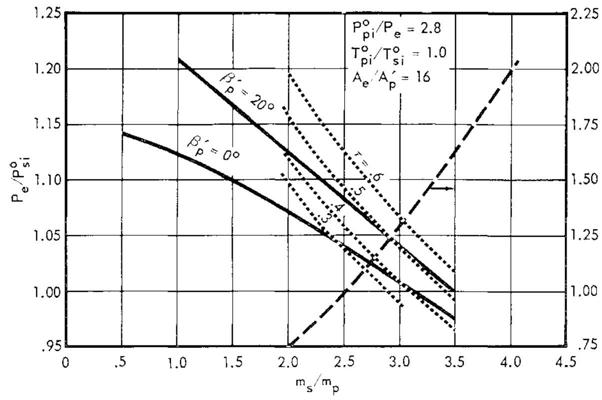

Fig. 3a) Analytical operating lines, temperature ratio of 1.

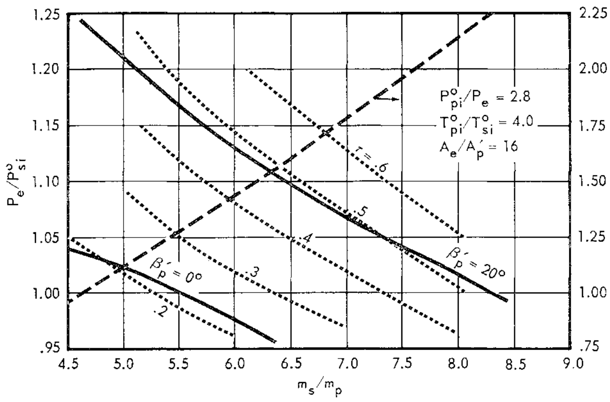

Fig. 3b) Analytical operating lines, temperature ratio of 4.

p_e/p_{si}^0 vs mass flow ratio m_s/m_p. Such plots for constant efficiency can be easily developed from Eqs. (5, 8, 9, and 10). If a chart with constant efficiency lines is used to plot experimental or analytical operating lines, the efficiency for each mass flow ratio can be immediately read on the diagram (Fig. 3), which will be discussed in Sec. 5.

2.3 Thrust Augmentation

Assuming that the primary gas, before being energized in a gas generator, has the same freestream velocity v_s' as the secondary flow, the total thrust of the augmenter is from the momentum equation

$$F = m(v_e - v_s')$$

The reference thrust is

$$F_p' = m_p(v_p' - v_s')$$

The thrust augmentation ratio is, therefore,

$$F/F_p' = [\bar{m}(\bar{v}_e - \bar{v}_s')]/[1 - \bar{v}_s'] \tag{11}$$

This equation contains the same quantities as Eq. (8) defining the efficiency, so that a direct relation between τ and F/F_p' exists. For augmenters, it is practical to plot the thrust augmentation ratio F/F_p' vs the freestream velocity ratio v_s'/v_p'. For constant efficiency τ such plots can be easily developed from Eqs. (5, 8, and 11). An example is shown in Fig. 4 for a primary pressure ratio of $p_{pi}^0/p_e = 2.8$, an inlet temperature ratio of $T_{pi}^0/T_{si}^0 = 4$, an efficiency $\tau = 0.5$, and three area ratios $A_e/A_p' = 5$, 10, and 20. Also shown in Fig. 4 are the corresponding mass flow ratio curves. Contrary to a common belief, an increase in area ratio and thereby mass flow ratio improves the thrust augmentation not only at static operation but also at high freestream velocities. Figure 4 is only concerned with internal losses and does not account for the external aerodynamic drag of the device. Approximately constant efficiency can only be expected if duct choking is avoided.

At zero freestream velocity v_s', Eq. (11) reduces to the expression for static thrust augmentation

$$F/F_p' = [(m_s/m_p) + 1]v_e/v_p' \tag{12}$$

which is plotted as dash curves in Fig. 2 for the two indicated inlet total temperature ratios. The static thrust augmentation curves of Fig. 2 apply only to that particular mass flow ratio for which the exit static pressure is equal to the total inlet secondary pressure. In order to use the thrust augmentation curves of Fig. 2, it is therefore necessary to know the operating line of p_e/p_{si}^0 vs m_s/m_p either from an analysis or from tests.

3. Principle of Flow Induction by Rotary Jets

Figure 1, which is taken from Foa,[2] shows schematically the rotary jet flow inductor. The primary gas is discharged from a number of nozzles in the rotating central streamlined body into an interaction region outwardly bounded by a nonrotating cylindrical duct. The nozzles are arranged in such a way that the direction of the exhaust velocity in the rotor-fixed reference system is not purely axial but has a tangential component. The tangential reaction of the primary jets spins the rotor and thereby causes the primary gas to form a spiral pattern as indicated by the dotted region in Fig. 1. Seen from the duct-fixed reference system, this primary gas spiral moves in the downstream direction carrying the secondary flow in between with it. Since the rotor does not resist the rotational motion except for a small bearing and aerodynamic surface friction, the angular momentum of the primary gas in the duct-fixed reference system is initially close to zero; that is before its interaction with the secondary gas. The primary gas particles, although arranged in the spiral pattern shown in Fig. 1, have initially, in the duct-fixed reference system, only a small tangential velocity component, which is taken as negligible in this analysis.

For the purpose of visualizing the interaction flow pattern, it is assumed that the interaction region between duct and centerbody is a thin cylindrical ring, so that the flow veloci-

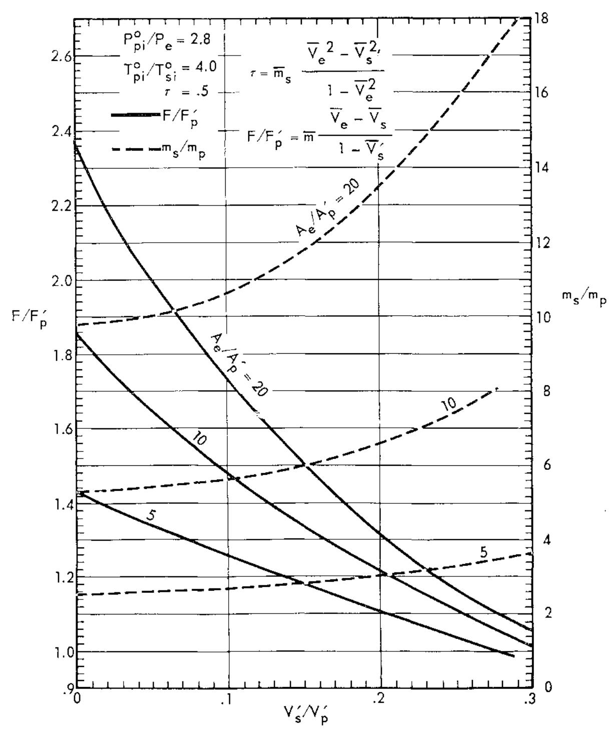

Fig. 4 Thrust augmentation ratio and mass flow ratio.

ties have no radial components and are uniform along any radius inside the ring. It should be noted, however, that the analysis in the subsequent section is not restricted to this special case. The tangential rotor speed in the center of the thin interaction ring section is v_t. The flow pattern is best visualized in a rotor-fixed frame of reference since it is steady in such a frame, whereas it is unsteady in a duct-fixed coordinate system. Developing the ring layer into a plane, one will get a flow pattern schematically shown in Fig. 5. The primary jet is discharged from a nozzle N at an oblique angle to the direction A-A of the rotor axis. The secondary flow enters the merging region at a larger angle, since its axial velocity component is smaller, and its tangential velocity component v_t is the same as for the primary jet. The two flows experience a "glancing collision" after which their average velocities u_p and u_s have the same direction, indicated in Fig. 5 by the angle β. Although Fig. 5 shows that at the merging station the secondary flow velocity is far from uniform, it is assumed that after mutual deflection into the common direction β the flows are sufficiently uniform so that u_p and u_s can be considered approximately equal both to the velocity average and to the square root of the velocity square average. The two average velocities u_p and u_s will be, however, of substantially different magnitude.

Since no tangential momentum is added to the flows anywhere in their passage through the device, the total tangential momentum of the flows after their mutual deflection into a common direction must be zero in the duct-fixed frame of reference, which means that the tangential momentum is mv_t in the rotor-fixed frame of reference. If the total linear momentum in the direction β is denoted by mu_d, and its axial component is denoted by mv_d, the tangential momentum condition can be expressed by the equations

$$mu_d = m_p u_p + m_s u_s \qquad (13)$$

$$v_d^2 = u_d^2 - v_t^2 \qquad (14)$$

The angle β for the common direction is obtained by either

$$\sin\beta = v_t/u_d \qquad (15)$$

or by

$$\cos\beta = v_d/u_d \qquad (16)$$

As can be seen from the schematic picture of Fig. 5, the interaction flow pattern is rather complicated. The details of this interaction flow will be disregarded in the following analysis, which will be merely based on the assumption that the flows in a rotor-fixed frame of reference are steady and isentropic. This assumption, together with the tangential

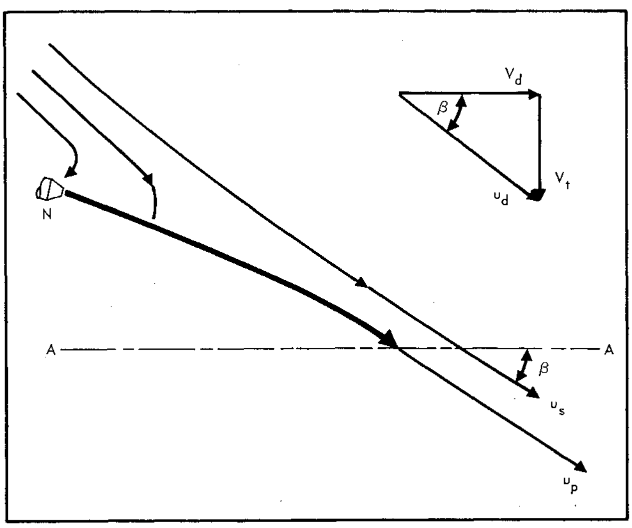

Fig. 5 Schematic interaction flow pattern in rotor-fixed frame of reference.

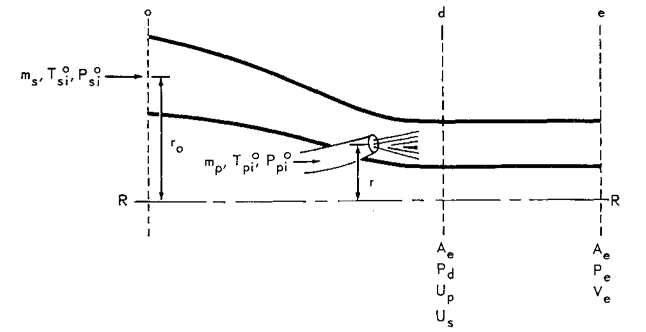

Fig. 6 Model for flow induction analysis.

momentum condition expressed in Eqs. (13) and (14), is sufficient to determine the performance of the flow inductor. Obviously, such an analysis can only give an upper limit for the performance, since the actual flows will not be exactly isentropic.

The analysis will show that the rotary jet flow inductor with isentropic flow deflection followed by constant area mixing is capable of substantially better performance than the ideal ejector with the same geometry. There is a widely held opinion that the ideal ejector represents the optimum for any steady flow induction process; and it is well known, for example, that a constant area mixing duct, when operated as a static augmenter with incompressible fluids, cannot provide more than a thrust augmentation ratio of 2, a value that is only asymptotically reached for infinitely large ratio of secondary over primary mass flow. The usual assumptions for the analysis of the ideal ejector are that the two flows are uniform at the merging station. If, in addition, the exit flow is assumed to be perfectly mixed, axial momentum balance and conservation of mass are sufficient to uniquely compute the performance of the ejector. There thus appears to be no room for improvements. However, as is indicated by Fig. 5, isentropic collision of two flows requires a nonuniform velocity distribution at the merging station, which makes the conventional ejector equations inapplicable and explains why the rotary jet inductor can have a substantially better performance than the ejector of equal geometry.†

4. Analysis of the Ideal Rotary Jet Flow Inductor

Following the isentropic mutual flow deflection in the rotor-fixed frame of reference, the two flows will be assumed to mix at constant area, so that the analysis reduces to that of the constant area ejector when the rotational speed of the primary jets is zero. In practical applications it is often of advantage to provide a diffuser before discharging the mixed flows. This is true, for example, if the flow induction device is to be used as a static thrust augmenter. The analysis of the effects of a diffuser and its optimization to suit a particular operational condition is the same whether or not the primary jets are rotating. Diffuser effects have, therefore, been omitted in the following study. It should be kept in mind, however, that the efficiencies and augmentation ratios obtained from the analysis have only relative significance and can be substantially modified by an added diffuser.

Figure 6 shows the model for the flow induction analysis; R-R is the rotor axis. Station o refers to the freestream location, station d is at the end of the mutual flow deflection and at the beginning of the constant area mixing section, and station e refers to the exit. The primary flow with the inlet conditions T_{pi}^0, p_{pi}^0 is assumed to be injected at the radial distance r from the rotor axis. The secondary flow with the

† The reasoning in this paragraph was first used in a personal letter by Foa after the author had pointed out contradictions connected with the prerotation assumption in Foa.[2,4]

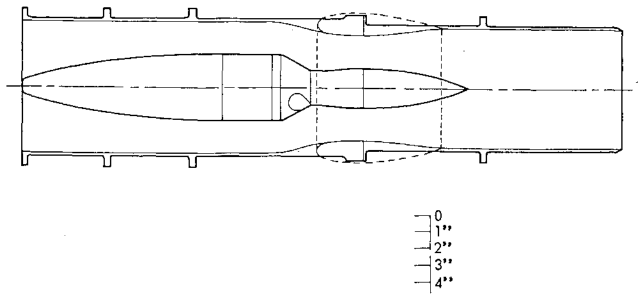

Fig. 7 Contours of rotor and duct.

inlet conditions T_{si}^0, p_{si}^0 is assumed to have at station o the radial distance r_0 from the rotor axis, and at stations d and e the radius r, the same as the primary flow. The thickness of the flow layer is assumed to be sufficiently small to justify a radially uniform velocity distribution in the analysis flow model. The changes of state between stations o and d are assumed to be isentropic. In addition to the flow variables shown in Fig. 6, there is the tangential speed v_t of the primary nozzles located at the radius r. The nondimensional tangential velocity can also be written in terms of the equivalent spin angle β_p'

$$\bar{v}_t = v_t/v_p' = \tan\beta_p' \tag{17}$$

which will be used in presenting the results of the analysis. The equivalent spin angle β_p' will in general be approximately equal to the geometric nozzle spin angle. However, tangential rotor drag or shock or Coanda deflections of the primary jets from the direction of the nozzle axes, together with the effects of the merging static pressure on the jet velocity, may produce some deviations between the nozzle spin angle and the equivalent spin angle β_p' as defined by Eq. (17).

At the end of deflection station d, the velocities u_p and u_s taken in the rotor-fixed reference system have the same direction. The temperatures T_p and T_s apply to both the rotor-fixed and the duct-fixed reference system.

The primary flow energy equation between inlet and station d reads in the rotor-fixed reference system

$$u_p^2/2c_p = T_{pi}^0 + (v_t^2/2c_p) - T_p$$

and assumes, with $v_p'^2/2c_p = T_{pi}^0 - T_{pe}'$, the nondimensional form

$$\bar{u}_p^2 = \bar{v}_t^2 + (\bar{T}_{pi}^0 - \bar{T}_p)/(\bar{T}_{pi}^0 - 1) \tag{18}$$

where the temperature T_p is obtained from the isentropic relation

$$T_p/T_{pi}^0 = (p_d/p_{pi}^0)^{(\gamma-1)/\gamma} \tag{19}$$

The secondary flow energy equation between stations o and d reads, in the rotor-fixed reference system,

$$u_s^2/2c_p = T_{si}^0 + (v_{t0}^2/2c_p) - T_s + (\Phi_0 - \Phi)/c_p \tag{20}$$

where Φ_0 and Φ are the potential energies of the centrifugal field:

$$\Phi_0 = -(v_{t0}^2/2) \qquad \Phi = -(v_t^2/2) \tag{21}$$

Inserting Eq. (21) into Eq. (20) and nondimensionalizing the same way as before, one obtains

$$\bar{u}_s^2 = \bar{v}_t^2 + (\bar{T}_{si}^0 - \bar{T}_s)/(T_{pi}^0 - 1) \tag{22}$$

The freestream tangential velocity v_{t0} has cancelled out of the energy equation. The temperature T_s follows from the isentropic relation

$$T_s/T_{si}^0 = (p_d/p_{si}^0)^{(\gamma-1)/\gamma} \tag{23}$$

Equations (18–23) determine the absolute values of the deflected velocities. The direction of these velocities is obtained by $\cos\beta = v_d/u_d$ (Fig. 5) where, according to Eqs. (13) and (14),

$$\bar{u}_d = (m_p/m)\bar{u}_p + (m_s/m)\bar{u}_s \tag{24}$$

$$\bar{v}_d = (\bar{u}_d^2 - \bar{v}_t^2)^{1/2} \tag{25}$$

The axial velocity components after deflection are

$$\bar{v}_{pd} = \bar{u}_p(v_d/u_d) \qquad \bar{v}_{sd} = \bar{u}_s(v_d/u_d) \tag{26}$$

and the axial flow area is

$$\bar{A}_e = (1/\bar{v}_{pd})\rho_p'/\rho_{pd} + (1/\bar{v}_{sd})(\rho_p'/\rho_{sd})m_s/m_p \tag{27}$$

where

$$\rho_p'/\rho_{pd} = (p_e/p_d)\bar{T}_p \qquad \rho_p'/\rho_{sd} = (p_e/p_d)\bar{T}_s \tag{28}$$

The static pressure increment through the mixing duct from station d to station e is obtained by the axial momentum equation:

$$m_p[u_p(v_d/u_d) - v_e] + m_s[u_s(v_d/u_d) - v_e] = A_e(p_e - p_d)$$

By making use of Eqs. (24) and (25) and by nondimensionalizing, one obtains

$$(m/m_p)\,(\bar{v}_d - \bar{v}_e) = (\bar{A}_e/2)\,(\bar{p}_e - \bar{p}_d) \tag{29}$$

One way of numerically solving the preceding set of equations is to assume as given the primary and secondary flow inlet variables $m_pT_{pi}^0p_{pi}^0$, $m_sT_{si}^0p_{si}^0$; the static exit pressure p_e; and the spin angle $\beta_p'i$. In order to evaluate Eqs. (18, 19, 22, and 23), one assumes a trial value for p_d. The area ratio $\bar{A}_e$ can then be determined from Eq. (27), the exit velocity ratio $\bar{v}_e$ from Eq. (5); and Eq. (29) serves as a check for the assumed trial value of p_d.

In many cases the pressure increment $p_e - p_d$ in the mixing section is small as compared to p_e and to $(p_{pi}^0 - p_e)$. It is then approximately $\bar{T}_p = 1$, and Eqs. (18) and (19) reduce to

$$\bar{u}_p^2 = \bar{v}_t^2 + 1 \tag{30}$$

The pressure ratio p_d/p_{si}^0 rather than the pressure p_{si}^0 can now be introduced as an independent variable, which allows the evaluation of Eqs. (22–26). The area ratio is approximately

$$\bar{A}_e = 1/\bar{v}_{pd} + (\bar{T}_s/\bar{v}_{sd})m_s/m_p \tag{31}$$

The exit velocity ratio $\bar{v}_e$ follows again from Eq. (5), and $\bar{p}_e - \bar{p}_d$ from Eq. (29). Since

$$\bar{p}_e - \bar{p}_d = (p_e - p_d)/\tfrac{1}{2}p_e\gamma M_p'^2 = [1 - (p_d/p_e)]/\tfrac{1}{2}\gamma M_p'^2$$

one can now compute

$$p_e/p_{si}^0 = p_d/p_{si}^0 \cdot p_e/p_d$$

directly without a trial and error process. The operating line of the flow induction device p_e/p_{si}^0 vs m_s/m_p can now be determined for constant area ratio $\bar{A}_e$ by suitable cross plotting.

5. Numerical Example

Figure 3 shows the operating lines for a primary pressure ratio of $p_{pi}^0/p_e = 2.8$, an area ratio of $A_e/A_p' = 16$, and equivalent spin angles of $\beta_p' = 0°$ and $20°$.‡ Figure 3a is for a temperature ratio of $T_{pi}^0/T_{si}^0 = 1$, and Fig. 3b is for $T_{pi}^0/T_{si}^0 = 4$. The lines of constant efficiency, determined according to Sec. 2, are shown in light dash lines. The static

‡ The curves are computed with Eqs. (30) and (31). Spot checks with the exact method showed small increases in pressure ratio for given mass flow ratio.

thrust augmentation ratio (heavy dashed line) is taken from Fig. 2. In the comparison of Figs. 3a and 3b, it is evident that for a given secondary pressure ratio p_e/p_{si}^0 and for a given area ratio A_e/A_p', hot primary gas draws a much higher secondary mass flow per unit primary flow. Nevertheless, the efficiency of the ejector ($\beta_p' = 0$) is lower for the hot primary gas, the reason being that the entropy increase from mixing is greater. On the other hand, Figs. 3a and 3b show that for the rotary jet flow inductor with a 20° equivalent spin angle the efficiency does not suffer from operation with hot primary gas.

The static thrust augmentation ratio is read in Fig. 3 by projecting the intersection of the operating line with the $p_e/p_{si}^0 = 1$ line upward onto the dash curve sloping to the right. Table 1 gives the static thrust augmentation ratios thus determined. Although hot primary gas, in spite of the increased secondary mass flow ratio, substantially reduces the static thrust augmentation of the ejector ($\beta_p' = 0$), it appreciably increases the thrust augmentation of the flow inductor with rotary jets. In other words, the effect of rotary jets, according to the isentropic theory, is very much greater for hot primary gas, since the increased mass flow ratio is not accompanied by a reduction in efficiency. Further numerical evaluation has shown that the primary pressure ratio, contrary to the temperature ratio, has only a relatively minor effect on the performance of the flow induction process, provided that choking within the device is avoided.

Model test results at equal primary and secondary total inlet temperatures have been obtained at the McDonnell Propulsion Laboratory and allow comparison with the preceding numerical example. Figure 7 shows the contours of the rotor and duct. Downstream of the merging station there is a short throat section followed by a rather steep-sloped diffuser, which is followed in turn by a constant area mixing section. The rotor has three nozzles of 1-in. diameter. The primary high-pressure air is ducted to the rotor through a strut not shown in Fig. 7. The low-pressure secondary air is pumped from the left to right through the flow interaction zone. Measured quantities are inlet total pressures and temperatures of the primary and secondary flow $p_{pi}^0\ T_{pi}^0\ p_{si}^0\ T_{si}^0$, mass flows m_p and m_s measured upstream of the flow inductor, rotor rpm, and exit static pressure. The equivalent spin angles β_p' from Eq. (17) are taken with the tangential rotor velocity in the center of the throat section.

Figure 8 shows the comparison of the measured operating lines for the four equivalent spin angles (0°, 14°, 18°, 24°) with analytical operating lines computed according to the equations of Sec. 4. As in the numerical example, the primary pressure ratio is $p_{pi}^0/p_e = 2.8$, and the area ratio is $A_e/A_p' = 16$. It is seen that, especially at lower mass flow ratios, flow induction by rotary jets yields a performance well above that of the ideal constant area ejector. The losses of the actual flow inductor, as compared to the ideal performance shown in the dash lines of Fig. 8, are partly from neglected wall friction, but probably are mainly from the neglected entropy increase during the deflection process. Spin angles higher than 24°, which theoretically should improve the performance further, could not be tested because of bearing difficulties at the high rotor rpm values.

The effect of mixing at constant area can be omitted in the analysis by assuming $p_e = p_d$ whereby Eq. (27) is simplified to Eq. (31), and Eqs. (5) and (29) are not needed. The mixing effect for the example of Fig. 3 is shown in Fig. 9. It is seen

Table 1 Static thrust augmentation ratios for the two equivalent spin angles and for two temperature ratios with $p_{pi}^0/p_e = 2.8$ and $A_e/A_p' = 16$

$T_{pi}^0/T_{si}^0 \rightarrow$	1	4
$\downarrow \beta_p'$		
0°	1.37	1.26
20°	1.63	2.25

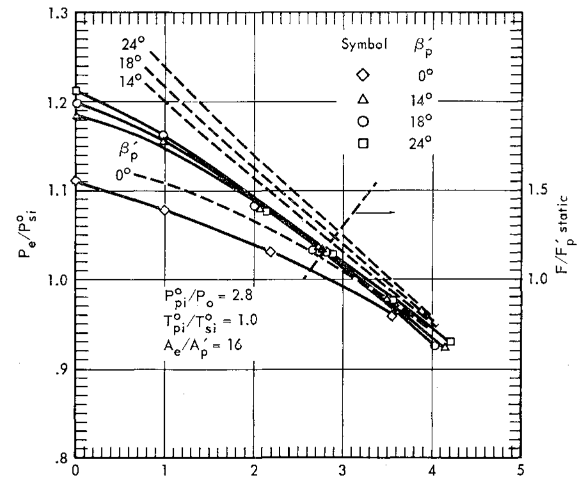

Fig. 8 Experimental (solid) and analytical (dash) operating lines.

that for equal total inlet temperatures mixing improves the performance, whereas it has the opposite effect at high primary gas temperature. The effect of mixing for equal total inlet temperatures has also been studied experimentally by removing the mixing duct to the right of the downstream flange shown in Fig. 7. Except for very low mass flow ratio m_s/m_p where a slight reduction in pressure ratio p_e/p_{si}^0 occurred, the removal of the mixing duct had no measurable effect on the performance. Some tests for which the thrust was measured by strain gauges were conducted with even shorter mixing length, as indicated in Fig. 7 by the dash line contours, again without measurable effect on the performance. Since, according to Fig. 8, the measured pressure ratio p_e/p_{si}^0 is considerably higher than that predicted in Fig. 9 for the case of no mixing, it must be concluded that rotary jet mixing can be accomplished within rather short mixing duct lengths.

At zero secondary mass flow, the equivalent to mixing is primary jet dissipation. Without such dissipation Fig. 9 shows, for 20° spin angle and for equal primary and secondary temperature, a pressure ratio of $p_e/p_{si}^0 = 1.12$, whereas even with the mixing duct removed the measured pressure ratio is over 1.20 (Fig. 8). This fact indicates that at zero secondary mass flow the rotary jets must dissipate rapidly within a short duct length.

6. Conclusions

The analysis of an idealized process of flow induction by rotary jets predicts for a typical example only a moderate performance improvement as compared to the constant area ejector, if the total inlet temperatures of the two flows are equal. The analysis predicts, however, a very substantial improvement if the primary gas total inlet temperature is four times that of the secondary gas.

Flow induction tests with equal inlet temperatures of the two gases confirm the trends of the analytical results. Mixing

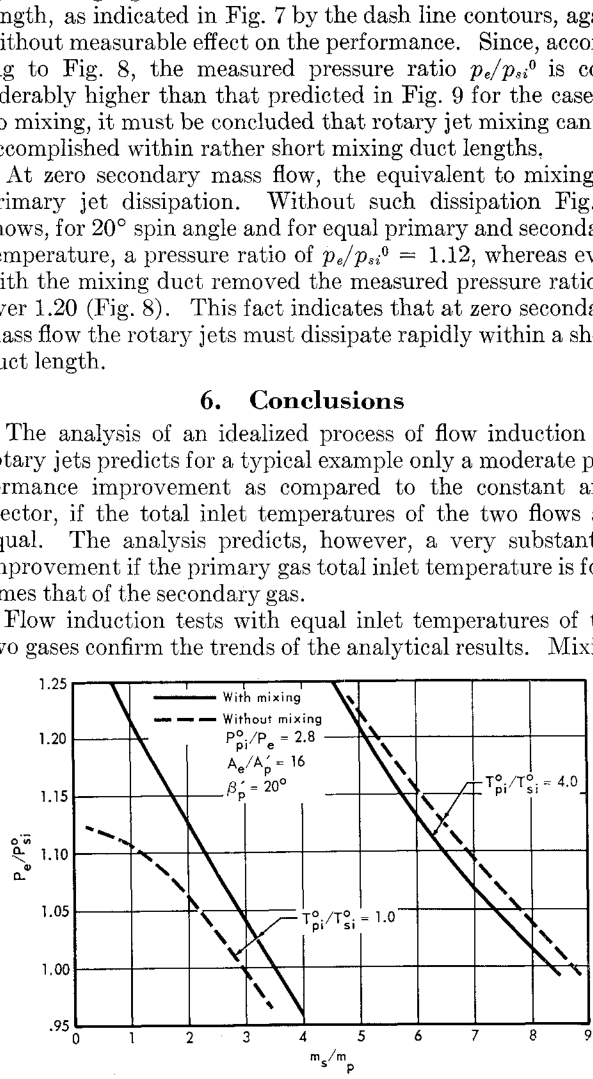

Fig. 9 Effect of mixing according to analysis.

of the rotary jets is achieved within short duct lengths. The reduction in performance as compared to the ideal device is probably mainly caused by the neglected jet dissipation during flow deflection.

Further progress in understanding and in evaluating the potential of flow induction by rotary jets should come with 1) a more sophisticated steady flow deflection analysis including jet dissipation and including three-dimensional flow effects, 2) steady flow deflection tests at various Mach number ratios and temperature ratios of the two flows and at various adverse static pressure gradients, and 3) rotary jet flow induction tests at elevated primary gas temperatures.

References

[1] Foa, J. V., "A new method of energy exchange between flows and some of its applications," Rensselaer Polytechnic Institute Aerospace Eng. TR AE 5509 (1955).

[2] Foa, J. V., "Crypto-steady pressure exchange," Rensselaer Polytechnic Institute Aerospace Eng. TR AE 6202 (1962).

[3] Foa, J. V., "A method of energy exchange," ARS J. **32**, 1396–1397 (1962).

[4] Foa, J. V., "A vaneless turbopump," AIAA J. **1**, 466–467 (1963).

[5] Hohenemser, K. H., "Preliminary analysis of a new type of thrust augmenter," *Proceedings of the 4th U. S. National Congress of Applied Mechanics* (American Society of Mechanical Engineers, New York, 1962), pp. 1291–1299.

[6] Cox, P. B. and Campbell, J. R., "Phase I summary technical report on advanced engine studies," Appendix VI-C, Marquardt Corp. Rept. 25,080, Vol. 2 (1963).

[7] McClintock, F. A. and Hood, J.H., "Aircraft ejector performance," J. Aeronaut. Sci. **13**, 559–568 (1946).

[8] Rabeneck, G. L., Shumpert, P. K., and Sutton, J. F., "Steady flow ejector research program," Lockheed Aircraft Corp., Georgia Div., Rept. ER-4708 (1960).

[9] Mitchell, J. W., "Design parameters for subsonic air-air ejectors," Stanford Univ., Dept. of Mechanical Engineering, TR 40 (1958).

[10] Traksel, J., "Simplified ejector and jet thrust augmentor theory," Lockheed Aircraft Corp., California Div., Rept. 14898 (1963).

[11] Payne, P. R., "Viscous mixing phenomena with particular reference to thrust augmentors," AIAA Preprint 64-798 (October 1964).